nature methods

Supplementary information

https://doi.org/10.1038/s41592-026-03174-y

Full-length single-cell spatial transcriptomics reveals spatial and cell-type-specific transcript isoforms in the primate brain

In the format provided by the authors and unedited

Table of Content

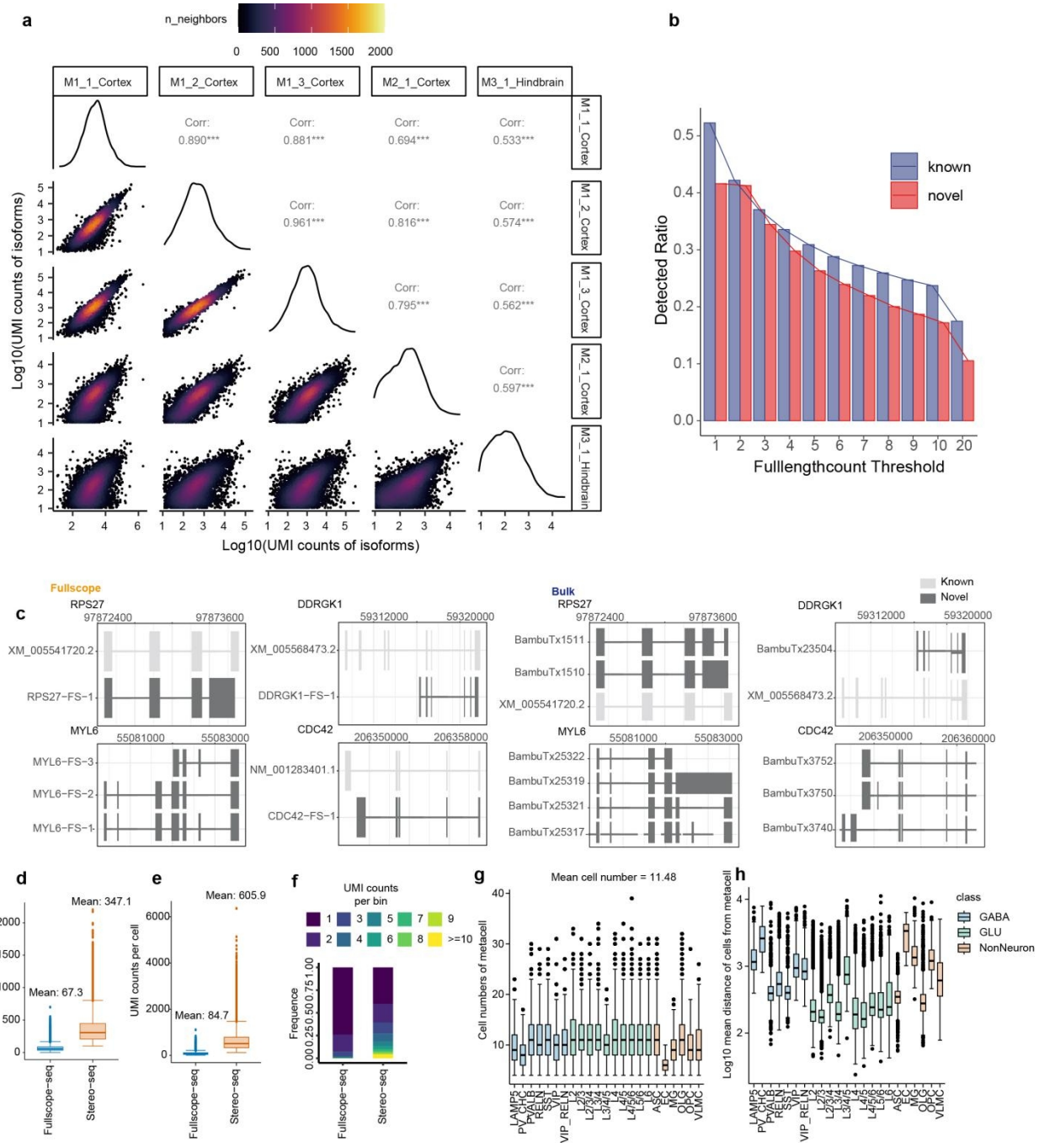

Supplementary Fig. 1 | Quality-control of Fullscope-seq. a, Correlation of isoform expression levels across biological replicates in the macaque brain, demonstrating high consistency within the same individual and between different individuals for cortical samples. **b,** Proportion of fullscope-seq transcripts validated in bulk long-read data across varying full-length read count thresholds. Transcripts were considered identical based on intron chain matches (i.e., identical splice junctions), irrespective of differences in transcription start or end sites. At a threshold of two full-length reads, both known and novel transcript detection rates exceed 40%. **c,** Validation in bulk data of transcripts associated with isoform-switch events identified by fullscope-seq in the original study. Transcripts corresponding to isoform-switching genes of interest—including *RPS27*, *DDRGK1*, *MYL6*, and *CDC42*—are consistently detected in independent bulk long-read

sequencing data from brain samples. **d**. Number of genes detected per cell; **e.** Average UMI counts per cell; **f.** UMI counts per spot, with the majority of spots containing a single cell; **g.** Histogram showing the number of cells assigned to each metacell; **h.** Distribution of intercellular distances within metacells**.** In each boxplot, the center line indicates the median, the lower and upper hinges indicate the first and third quartiles, and the whiskers extend to 1.5 × IQR.

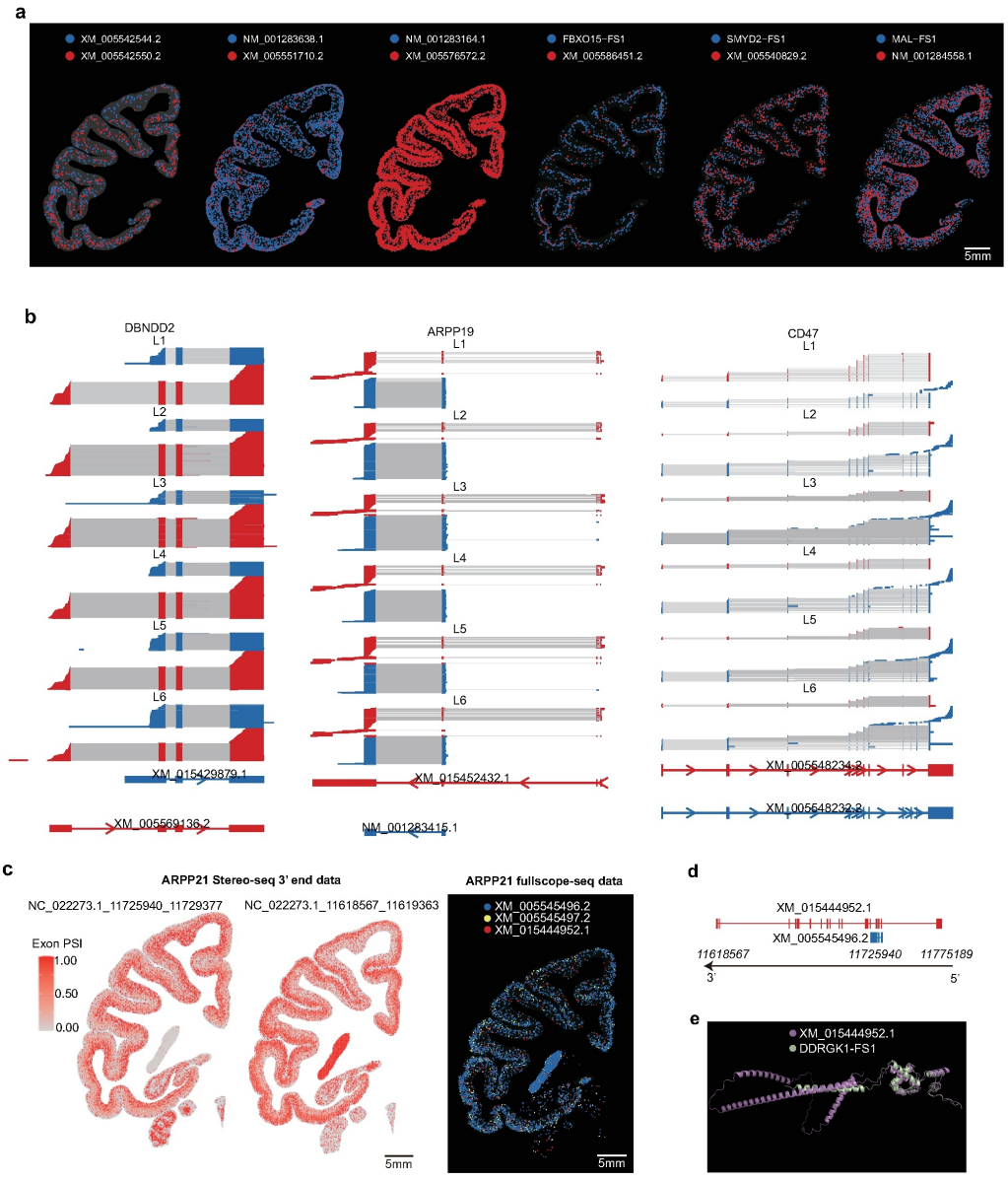
a
XM_005542544.2
XM_005542550.2
NM_001283638.1
XM_005551710.2
NM_001283164.1
XM_005576572.2
FBXO15-FS1
XM_005586451.2
SMYD2-FS1
XM_005540829.2
MAL-FS1
NM_001284558.1
5mm
b
DBNDD2
ARPP19
CD47
L1
L2
L3
L4
L5
L6
XM_015429879.1
XM_005569136.2
XM_015452432.1
NM_001283415.1
XM_005548234.3
XM_005548232.3
c
ARPP21 Stereo-seq 3' end data
NC_022273.1_11725940_11729377
NC_022273.1_11618567_11619363
Exon PSI
1.00
0.50
0.00
5mm
ARPP21 fullscope-seq data
XM_005545496.2
XM_005545497.2
XM_015444952.1
5mm
d
XM_015444952.1
XM_005545496.2
11618567
11725940
11775189
3'
5'
e
XM_015444952.1
DDRGK1-FS1

upplementary Fig. 2 | Isoform-level spatial patterns and validation in the macaque cortex. a, Isoform spatial pattern of reads of cortical layer marker genes in Fig. 2c. **b,** Splicing patterns of reads supporting DTU genes (*DBNDD2*, *ARPP19*, and *CD47*) across cortical layers. **c,** Comparison between Stereo-seq and fullscope-seq data illustrating 3'end usage of *ARPP21*. (Left) Spatial distribution of Percent Usage In values for two distinct terminal exons, with each point representing a 50-bin region. (Right) Spatial expression patterns of three major *ARPP21* isoforms. **d,** Structural annotation of *ARPP21* isoforms and their corresponding exons. The differential expression of two *ARPP21* isoforms with distinct terminal exons (TES) between deep and superficial cortical layers, as detected by fullscope-seq, aligns with the layer-specific expression of TES exons observed in Stereo-seq data, validating the reliability of thefullscope-seq approach. **e,** Predicted protein structure of two isoforms of *DDRGK1* by AlphaFold2. Green is the novel isoform DDRGK1-FS-1, red is isoform XM_005568473.2.

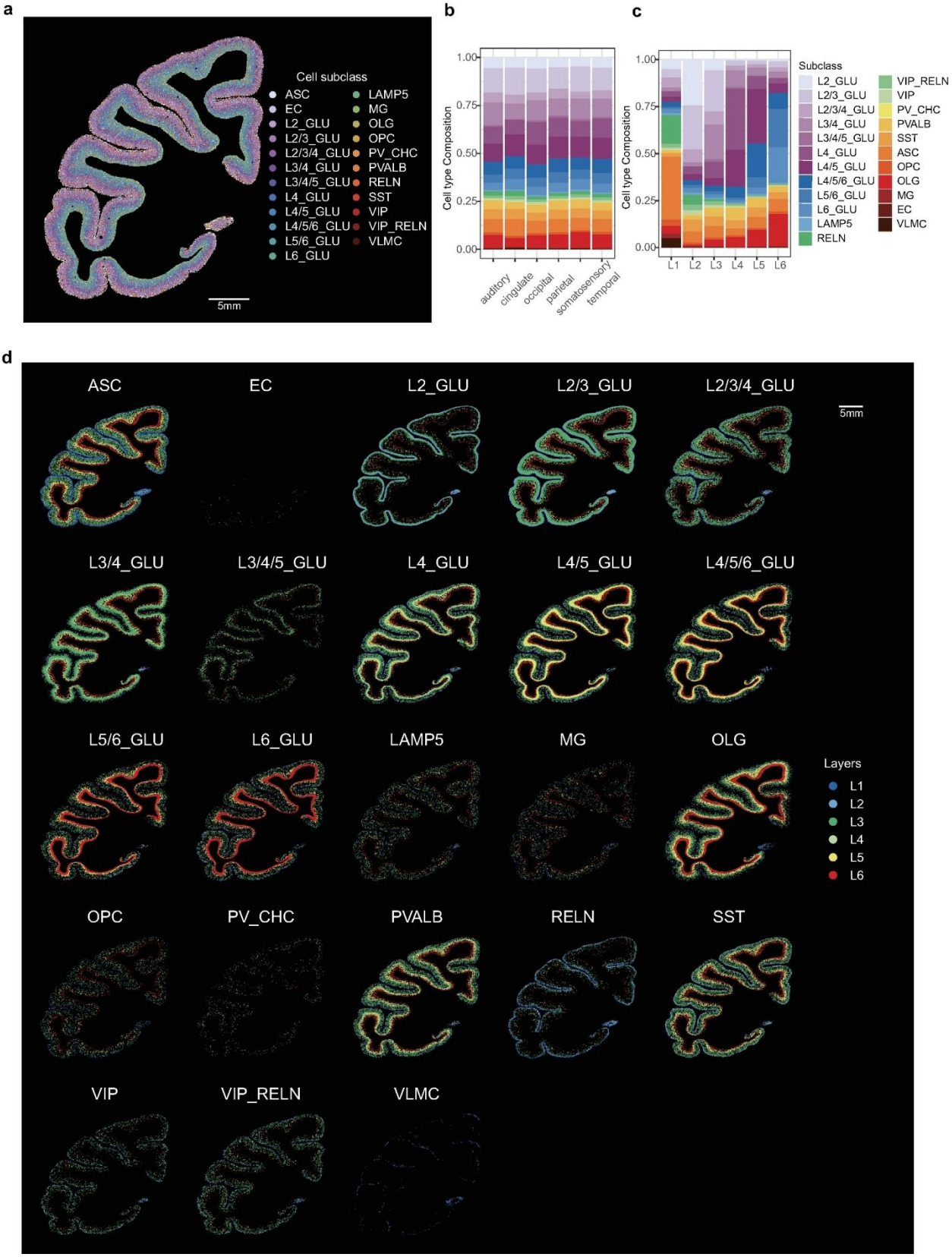
a
Cell subclass
ASC
EC
L2_GLU
L2/3_GLU
L2/3/4_GLU
L3/4_GLU
L3/4/5_GLU
L4_GLU
L4/5_GLU
L4/5/6_GLU
L5/6_GLU
L6_GLU
LAMP5
MG
OLG
OPC
PV_CHC
PVALB
RELN
SST
VIP
VIP_RELN
VLMC
5mm
b
Cell type Composition
1.00
0.75
0.50
0.25
0.00
auditory
cingulate
occipital
parietal
somatosensory
temporal
c
Cell type Composition
L1
L2
L3
L4
L5
L6
Subclass
L2_GLU
L2/3_GLU
L2/3/4_GLU
L3/4_GLU
L3/4/5_GLU
L4_GLU
L4/5_GLU
L4/5/6_GLU
L5/6_GLU
L6_GLU
LAMP5
RELN
VIP_RELN
VIP
PV_CHC
PVALB
SST
ASC
OPC
OLG
MG
EC
VLMC
d
ASC
EC
L2_GLU
L2/3_GLU
L2/3/4_GLU
5mm
L3/4_GLU
L3/4/5_GLU
L4_GLU
L4/5_GLU
L4/5/6_GLU
L5/6_GLU
L6_GLU
LAMP5
MG
OLG
Layers
L1
L2
L3
L4
L5
L6
OPC
PV_CHC
PVALB
RELN
SST
VIP
VIP_RELN
VLMC

Supplementary Fig. 3 | Cortical cell type spatial distribution of Macaque1-1. a, Subclass cell type annotation at spatial level. **b-c,** Subclass cell type proportion in different layers or lobes. **d,** Layer distribution of each subclass cell type.

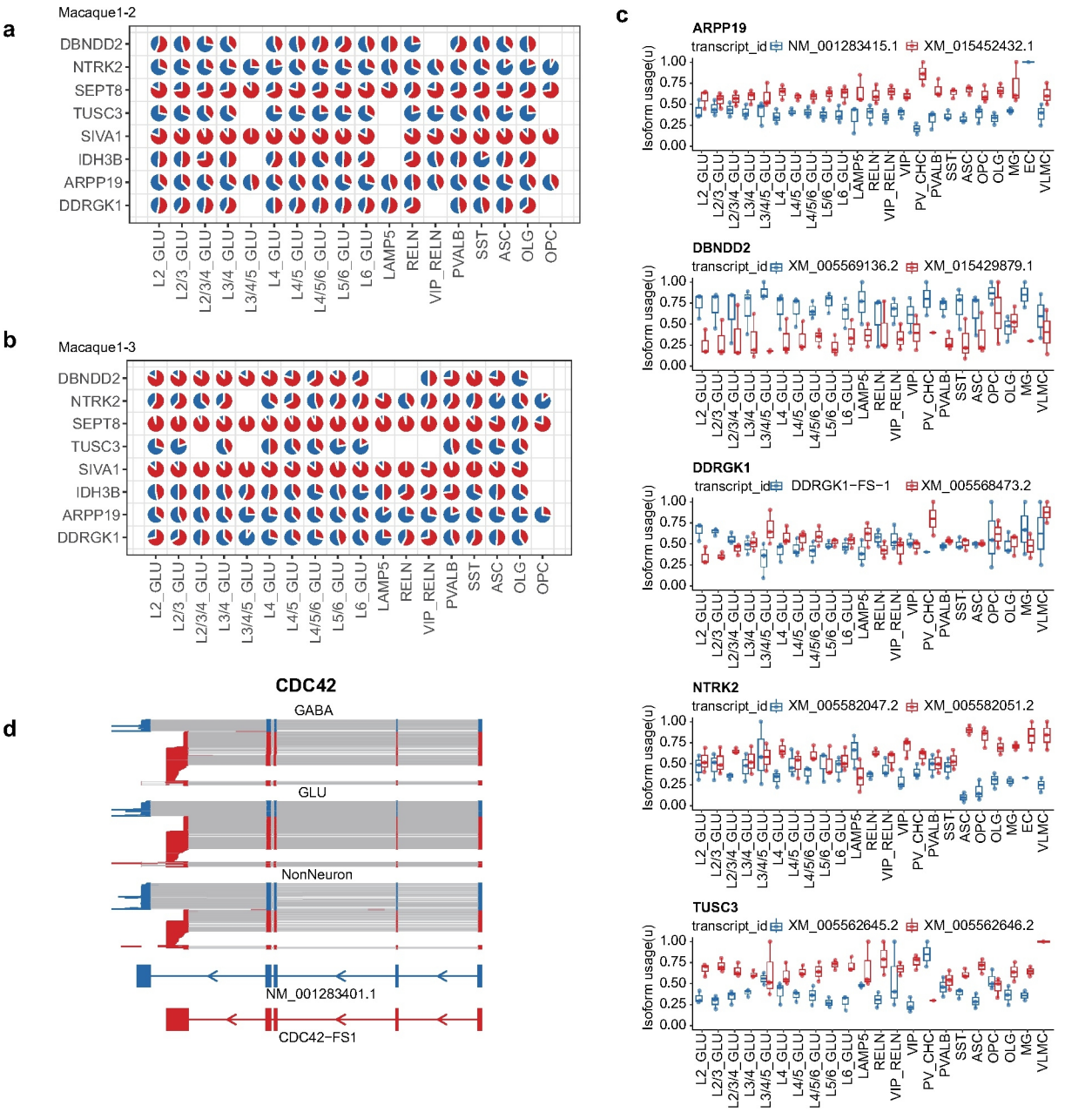

Supplementary Fig. 4 | Cortical Cell-type specific DTU cases in replicates. a-b, Isoform usage profiles of DTU genes across cell subclasses in Macaque1-2 (a) and Macaque1-3 (b), corresponding to Fig. 3e. Each pie chart represents the proportional usage of distinct isoforms for a single gene, with colors indicating isoform identity and a black outline highlighting isoforms involved in switching events. **c,** Isoform usage distribution of *ARPP19*, *DBNDD2*, *DDRGK1*, *NTRK2*, and *TUSC3* across three replicates (Macaque1 slices). the color of box represents different isoforms. The center line represents the median, the lower and upper hinges correspond to the first and third quartiles, and the whiskers extend to ±1.5× interquartile range (IQR). **d,** Splicing pattern of reads of *CDC42* across different cell classes in Macaque1-1. CDC42-FS-1 is a novel isoform with a different 3' ending site.

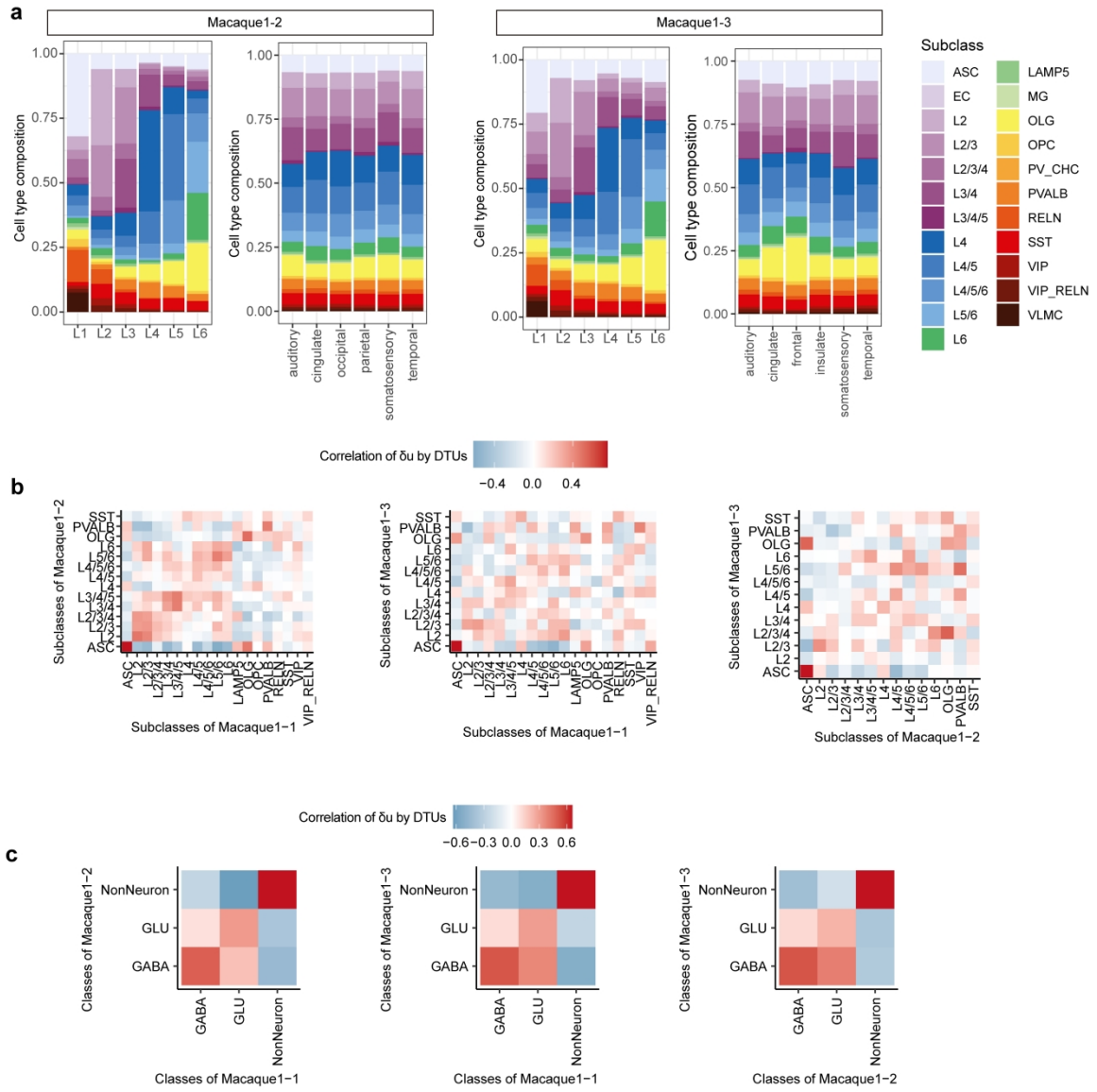

Supplementary Fig. 5 | Transcriptomic diversity and reproducibility of differential transcript usage across cortical cell types. a, Laminar distribution of cell subclass proportions in Macaque1-2 (left) and Macaque1-3 (right). **b,** Correlation of δu values for DTU events detected between cortical cell subclasses across biological replicates. **c,** Correlation of δu values for DTU events identified among cortical cell classes across replicates.

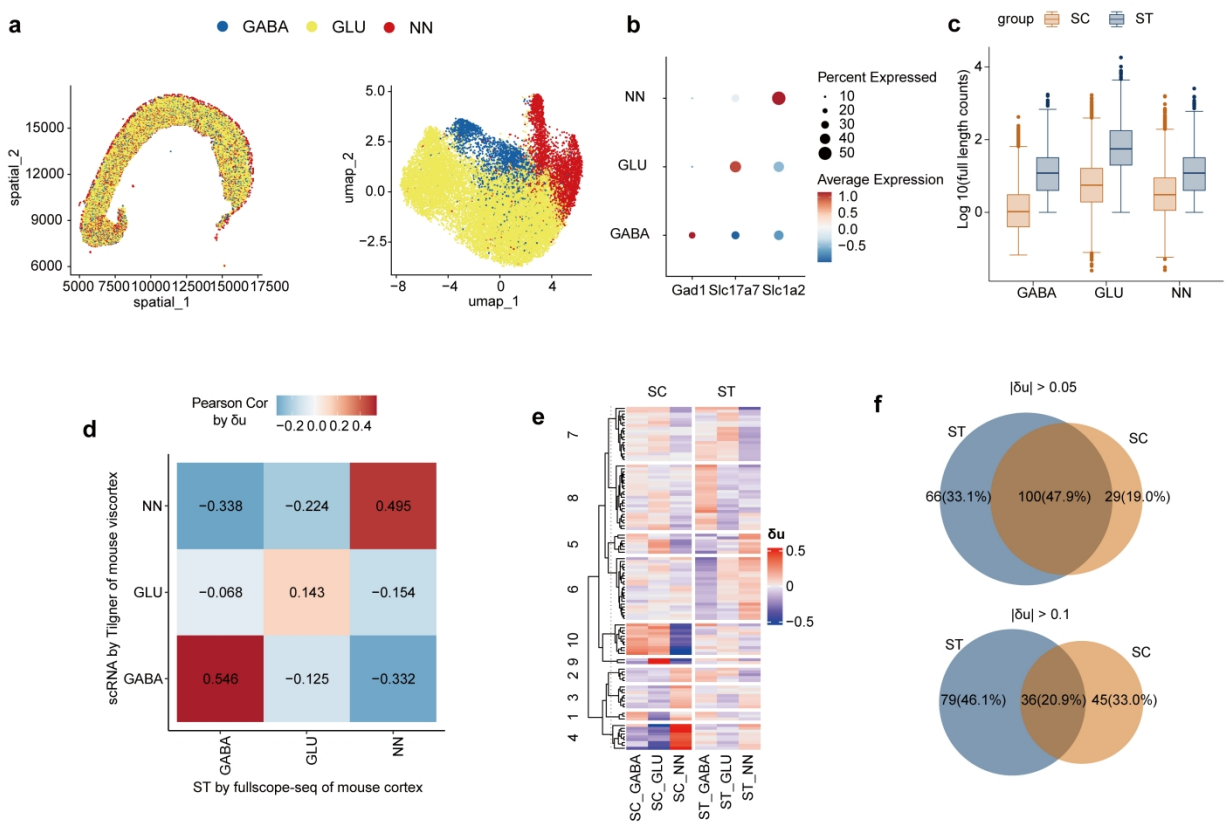

Supplementary Fig. 6 | Benchmarking of fullscope-seq reproducibility and sensitivity using datasets. a, Cell-type annotation and spatial visualization of a mouse cortex section profiled with Fullscope-seq. (Left) Spatial distribution of the corresponding cell types within the tissue section. (Right) UMAP projection of cells colored by annotated cell types. **b,** Expression of canonical marker genes for the identified cell types in the mouse Fullscope-seq data. **c,** Comparison of total full-length UMI counts per platform, showing that FullScope-seq achieves greater sequencing depth than the reference single-cell RNA-seq dataset (Joglekar et al., 2024)[2]. Each point represents an RNA isoform. A total of 22,271 isoforms are shown for single-cell RNA-seq (SC) and 2,643 isoforms for spatial transcriptomics (ST; FullScope-seq). In each boxplot, the center line denotes the median, the lower and upper hinges correspond to the first and third quartiles, and whiskers extend to 1.5× the interquartile range (IQR). **d,** Pearson correlation analysis of δu for isoforms detected in both the reference scRNA-seqand Fullscope-seq datasets. **e,** Hierarchical clustering of DTU δu values for isoforms assessed in both platforms, highlighting conserved and divergent isoform usage patterns. **f,** Overlap of significant DTU isoforms identified in both platforms, evaluated under varying δu thresholds.

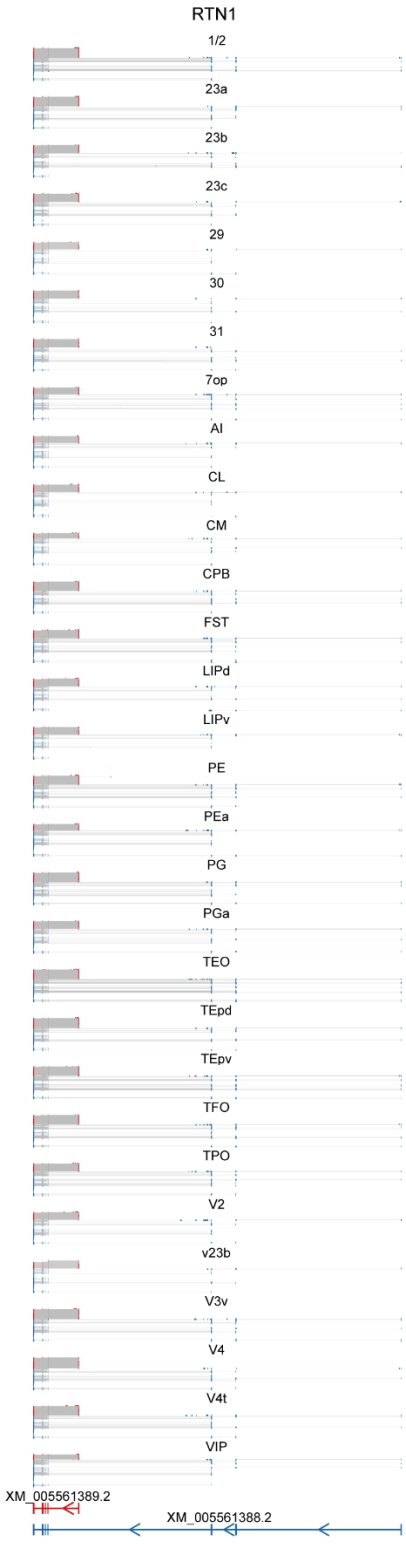

Supplementary Fig. 7 | Splicing pattern of reads of RTN1 across different cell subclasses.

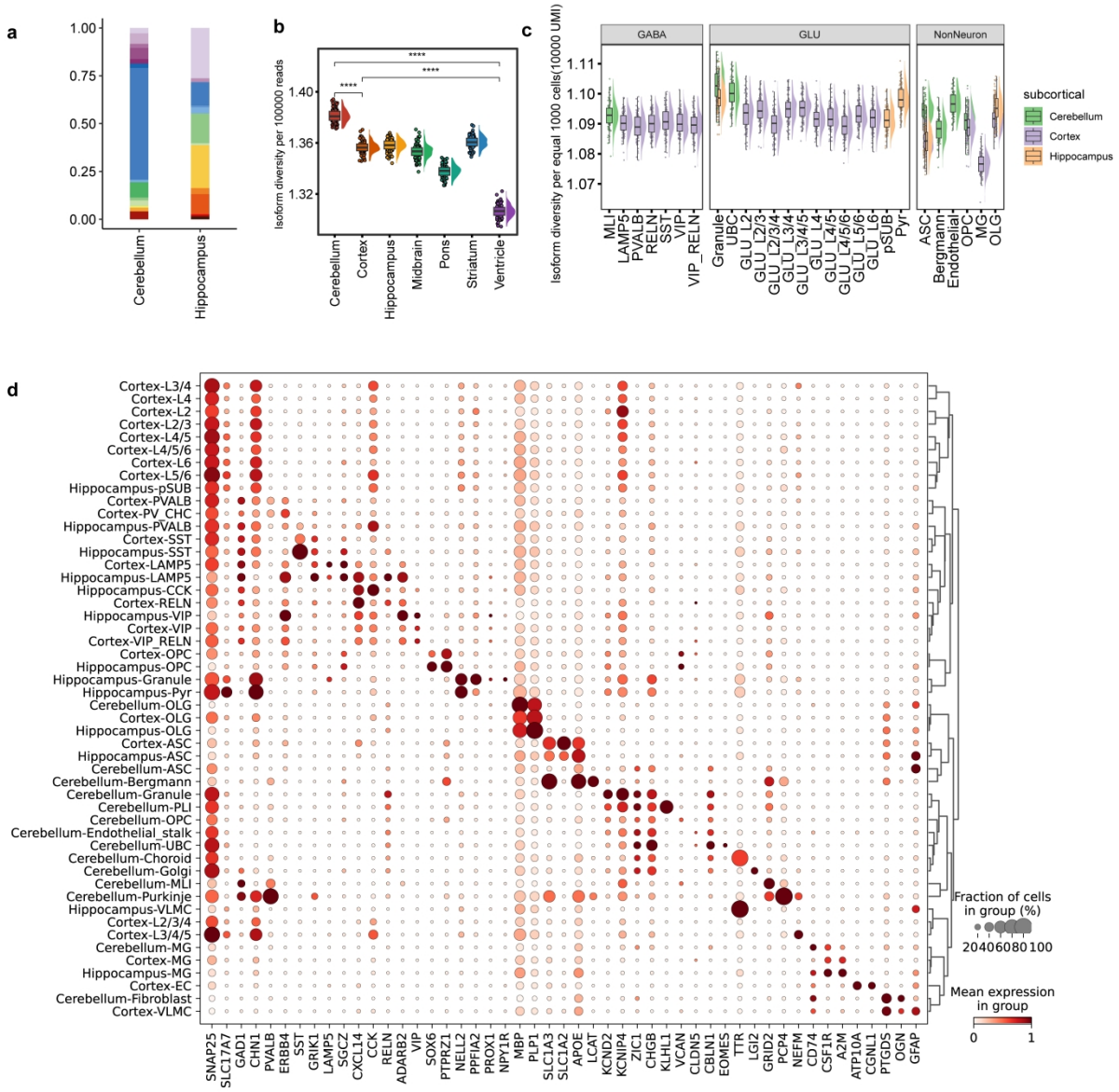

Supplementary Fig. 8 | Isoform diversity analysis and cell annotation across different brain regions. a, Cellular composition of the hippocampus and cerebellum in Macaque1-1, showing the proportional distribution of major cell types in each region. **b,** Regional variation in isoform diversity. The mean number of isoforms per gene was estimated after subsampling 100,000 UMIs per brain region 100 times to normalize sequencing depth. The cerebellum showed the highest isoform diversity among the regions analyzed, whereas the ventricle showed the lowest. In each boxplot, the center line indicates the median, the box bounds the first and third quartiles, and the whiskers extend to 1.5 × IQR. Statistical significance was determined using two-sided Student's t-tests with Holm correction for multiple comparisons. Significance was defined as ns, $P > 0.05$; *, $P \leq 0.05$; **, $P \leq 0.01$; ***, $P \leq 0.001$; and ****, $P \leq 0.0001$. The annotated comparisons were all significant: Cerebellum versus Cortex, adjusted $P = 2.4 \times 10^{-98}$; Cerebellum versus Hippocampus, adjusted $P = 6.2 \times 10^{-107}$; Cerebellum versus Striatum, adjusted $P = 1.3 \times 10^{-95}$; Cerebellum versus Ventricle, adjusted $P = 2.8 \times 10^{-187}$. **c,** Isoform diversity statistics of different cell subclasses. An equal number (500) of cells were randomly

selected from same cell types. Each point in the boxplot represents a single time of random sampling. Boxplot elements are defined as in panel b. **d,** Heatmap and hierarchical clustering of cell-type marker gene expression across regions, validating the accuracy of cell-type annotations. Cortical and hippocampal interneurons—including MGE-derived (PV^+, SST) and CGE-derived ($LAMP5^+$, VIP^+) subclasses—display highly concordant expression profiles.

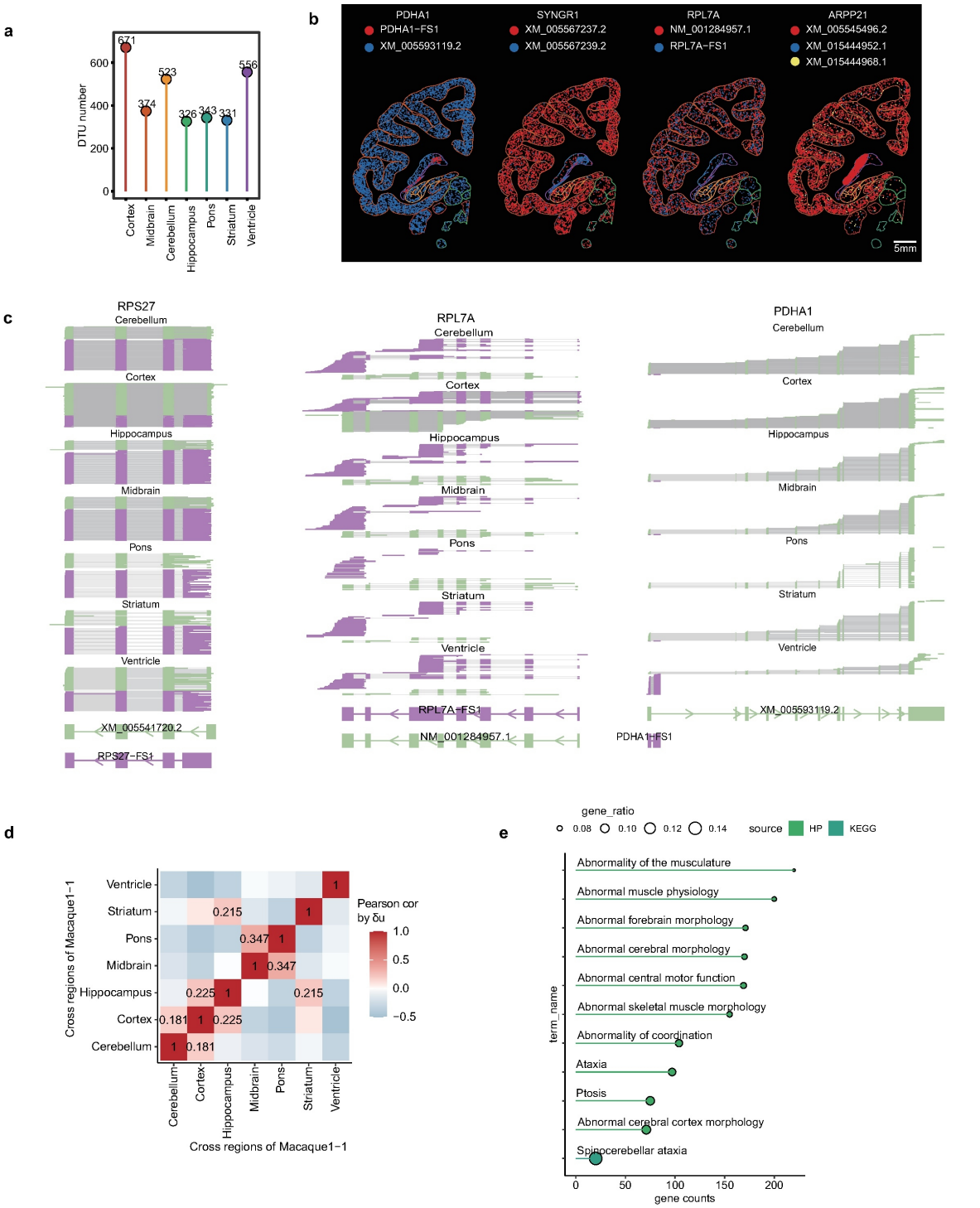

Supplementary Fig. 9 | Spatial heterogeneity and functional profiling of isoform diversity across brain regions. a, Number of brain region-specific DTU genes among different brain regions. Compared to other brain regions, cortex exhibits the highest number of DTU genes. **b,** Spatial plot of the DTU genes. Each point represents a single bin, and different colors indicate the dominant isoform type present in that bin. **c,** Splicing pattern of reads of DTU genes across different brain regions. **d,** Isoform similarity across brain regions, computed using δu values of DTU isoforms. **e,** Human phenotypes and KEGG analysis of DTU genes across brain regions.

Each row represents a term, color indicates different resources, and the size of the points represents the p-values from the enrichment test.

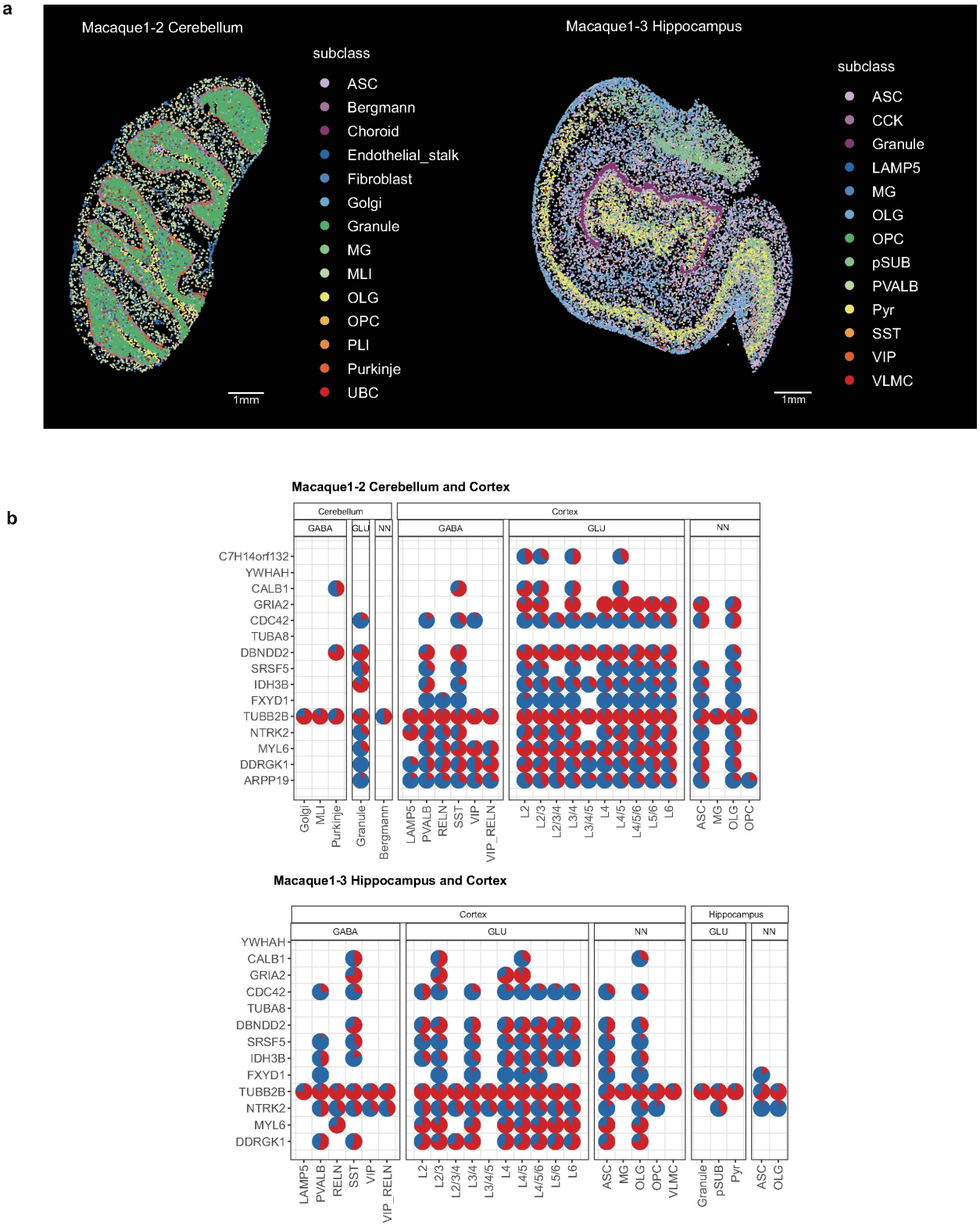

Supplementary Fig. 10 | Spatial cell-type annotation and reproducible DTU patterns in macaque cerebellum and hippocampus. a, Spatial annotation of cell types in the cerebellum (left) of Macaque1-2 and hippocampus (right) of Macaque1-3. **b,** Validation of DTU cases in the

cerebellum and hippocampus across biological replicates (Macaque1-2 and Macacaque1-3), showing high consistency with patterns observed in Macaque1-1.

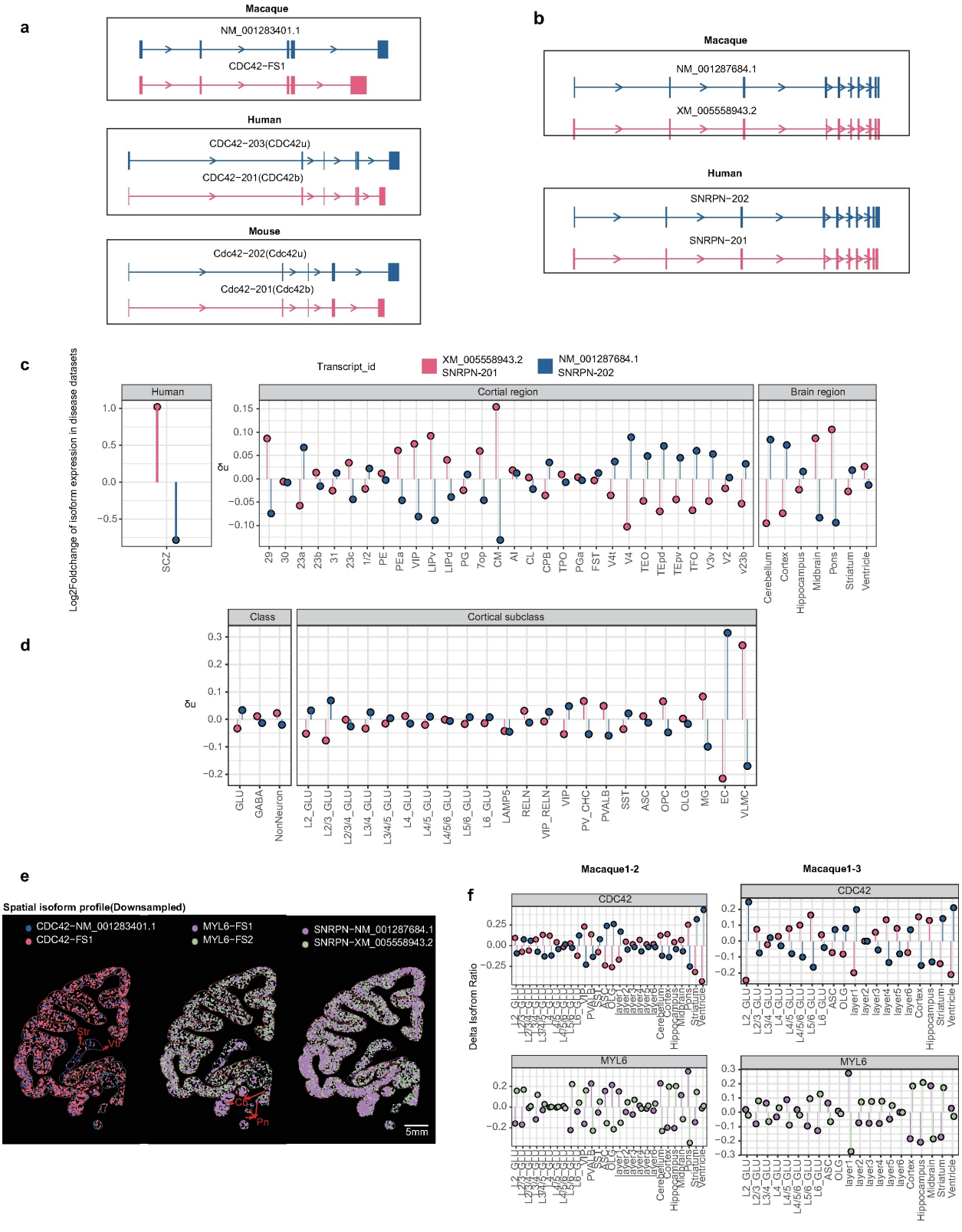

Supplementary Fig. 11 | Cross-species conservation and spatial expression of disease-associated differential transcript usage isoforms. a, Comparison of *CDC42* isoform structures

across species, with humans, mice, and macaque showing high similarity. **b,** Comparison of *SNRPN* isoform structures across species, with humans, mice, and macaque showing high similarity. **c-d,** Isoform usage patterns of *SNRPN* in human SCZ data and this study. Each color represents the presence of orthologous isoforms between macaques and humans. **e,** Spatial plot of *MYL6*, *SNRPN* and *CDC42*. Each point represents a single bin, and different colors indicate the dominant isoform type present in that bin. **f,** soform usage patterns for *CDC42* and *MYL6* in biological replicates Macaque1-2 and Macaque1-3. Color assignments are consistent with Fig. 6c.

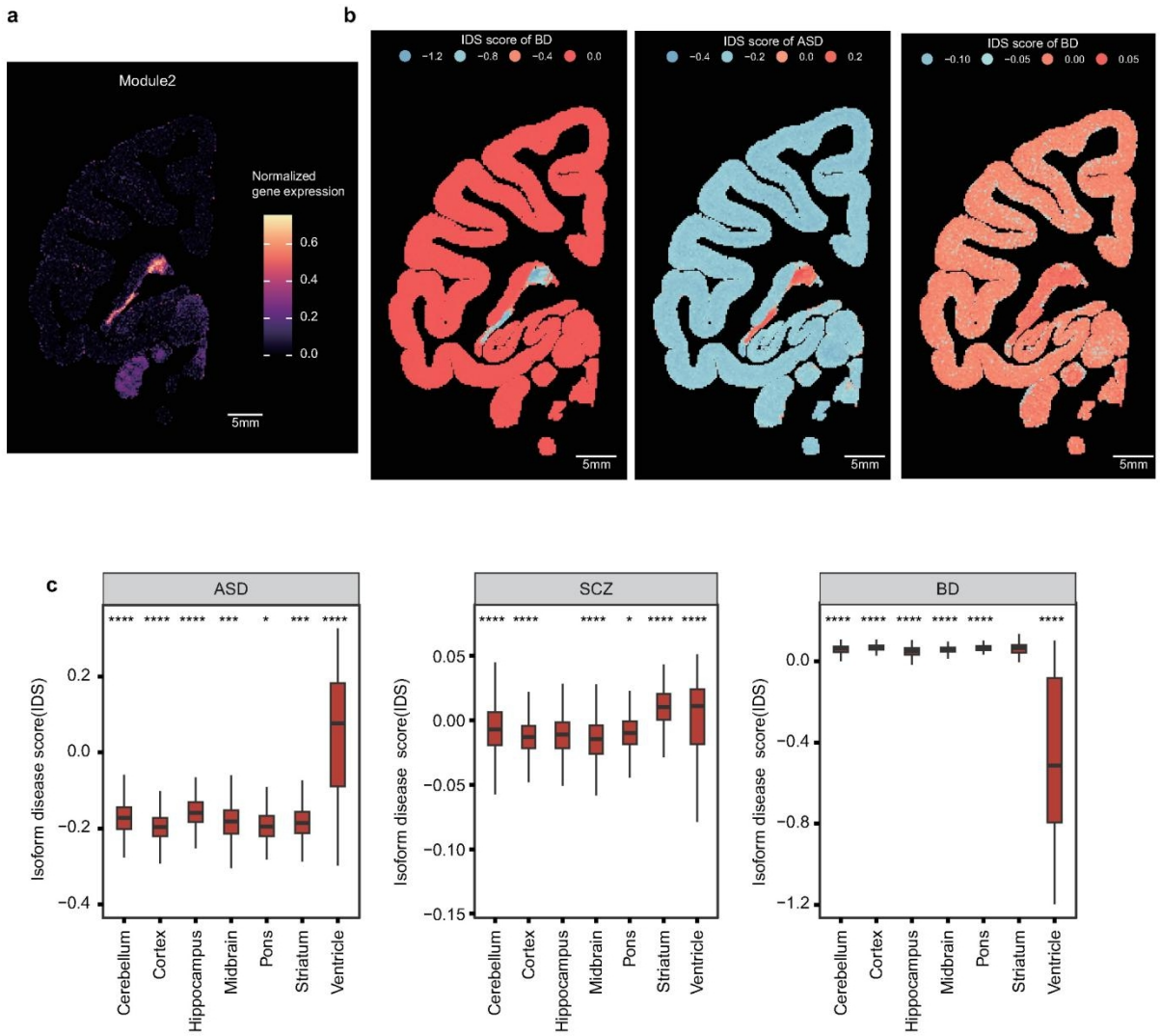

Supplementary Fig. 12 | Spatial function feature analysis with DTU isoforms. a, Spatial average expression of genes within Module 2. Genes in Module2 show spatial patterns similar to those of ventrical-specific DTU isoforms (e.g., *FXYD1*). **b,** Spatial distribution of the isoform disease score (IDS) for bipolar disorder (BD), schizophrenia (SCZ), and autism spectrum disorder (ASD). Each point corresponds to a spatial bin (bin size = 200), colored according to the IDS value, which reflects disease-associated changes in cross-species conserved isoform usage per bin. **c,** Summary of IDS distributions across brain regions, highlighting regional enrichment of disease-associated isoform usage patterns. Each unit represents a spatial bin (200 spots per bin). The numbers of bins were 716 for cerebellum, 10,479 for cortex, 449 for hippocampus, 754 for midbrain, 207 for pons, 322 for striatum, and 300 for ventricle. In each boxplot, the center line indicates the median, boxes indicate the first and third quartiles, and whiskers extend to 1.5 × IQR. P values were calculated using two-sided Student's t-tests, comparing each region with all other regions within each disorder. Significant differences were detected in all seven regions for ASD and SCZ, with exact P values as follows: ASD, cerebellum $P = 9.32 \times 10^{-20}$, cortex $P = 9.02 \times 10^{-69}$, hippocampus $P = 3.77 \times 10^{-59}$, midbrain $P = 5.04 \times 10^{-10}$, pons $P = 0.0494$, striatum $P = 1.57 \times 10^{-4}$, ventricle $P = 2.93 \times 10^{-86}$; SCZ, cerebellum $P = 1.35 \times 10^{-11}$, cortex $P = 6.74 \times 10^{-29}$, hippocampus $P = 4.10 \times 10^{-8}$, midbrain $P = 1.45 \times 10^{-4}$, pons $P = 1.49 \times 10^{-12}$, striatum P =

1.60×10^{-86}, ventricle $P = 2.60 \times 10^{-24}$. For BD, significant differences were observed in cerebellum ($P = 1.36 \times 10^{-12}$), cortex ($P = 5.98 \times 10^{-54}$), hippocampus ($P = 0.00463$), midbrain ($P = 1.20 \times 10^{-21}$), pons ($P = 1.94 \times 10^{-19}$), and ventricle ($P = 3.33 \times 10^{-71}$), whereas striatum was not significant. Significance was defined as *$P \leq 0.05$, **$P \leq 0.01$, ***$P \leq 0.001$, and ****$P \leq 0.0001$.